J Appl Electrochem (2012) 42:753–761
DOI 10.1007/s10800-012-0454-9

ORIGINAL PAPER

Patterned electrodeposition of interconnects using microcontact printing

A. Hovestad · H. Rendering · A. W. Maijenburg

Received: 15 February 2012 / Accepted: 6 July 2012 / Published online: 31 July 2012

Abstract Microcontact printing combined with electroless deposition is a potential low cost technique to make electrical interconnects for opto-electronic devices. Microcontact printed inhibitors locally prevent electroless deposition resulting in a pre-defined pattern of metal tracks. The inhibition of electroless Ni deposition on Pd-seeds and on indium tin oxide (ITO) by self-assembling molecules (SAM) was investigated. Polarisation measurements and transients show that on Pd seeds for electroless deposition, thiol-compounds inhibit the oxidation of the reducing agent, hypophosphite, in the electroless Ni bath. Cyclic voltammetry suggests that the inhibition is due to adsorption of the inhibiting molecules on active sites of the Pd-seeds only or as a SAM on the entire Pd seeds depending on the thiol-compound used. Polarization measurements show that after a pre-treatment in nitric acid hexadecylamine (HDA) is able to inhibit Ni electrodeposition on ITO. It was found that the pre-treatment activated ITO for Ni electrodeposition. Adsorbed HDA increases the crystallization overpotential for Ni electrodeposition by approximately 100 mV.

Keywords Microcontact printing · Electrodeposition · Self-assembling molecules · Thin film devices

1 Introduction

Thin film photovoltaic cells, organic light emitting diodes and thin film sensors are examples of opto-electronic devices integrating electrical and optical functionalities. Interconnection in optoelectronic devices is achieved by transparent conductive oxide (TCO), like indium tin oxide (ITO), aluminium doped zinc oxide (AZO) and fluor doped tin oxide (FTO). These materials combine a high optical transmission and a low electrical resistance. However, there is a trade-off between the electrical resistance and optical transmittance of TCOs. Therefore, high quality TCOs with a transmittance >90 % are limited to a >5 Ω/□ sheet resistance. For thin film solar cell it was shown in [1] that up to 25 % of resistive power losses can occur due to these limitations in TCO conductivity. For flexible opto-electronic devices obtaining high quality TCOs is even more challenging. Low-cost polymer materials, like polyethylene terephthalate (PET) and polyethylene naphthalate (PEN) are preferred as carrier foils for flexible thin film devices. The limited temperature resistance of polymers poses temperature restrictions on TCO deposition resulting in a lower conductivity or increased production costs. The low mechanical flexibility of the brittle ceramic TCO materials reduces the attainable TCO thickness and thereby the, thickness dependent, sheet conductivity of TCOs. Alternative transparent conductive films such as, graphene [2] and carbon nanotubes [3, 4] nano thin metal films [5–7] are being explored, but have not yet reached the optical and electrical performance of the best TCOs.

An alternative is to combine TCOs with a grid of high electrically conductivity metal lines. Metal grid electrodes can be combined with a TCO [7, 8], an organic transparent conductor [9–12] or an ultra thin metal film [13] have been investigated. The metal grids facilitate the current transport thereby relaxing the requirements on the TCO film conductivity. This allows the use of thinner and cheaper TCOs with higher optical transparency, flexibility in device design and improved durability by compensating for conductivity losses due to TCO degradation in time. Metal grids are typically

A. Hovestad (✉) · H. Rendering · A. W. Maijenburg
Expertise Group Thin Film Technology, TNO, P.O. Box 6235, 5600 HE Eindhoven, The Netherlands
e-mail: arjan.hovestad@tno.nl
URL: www.tno.nl

applied by screen or ink-jet printing of Ag particle based inks. However, in [7] it was shown that the highest conductivity transparent conductive layers, with a sheet resistance below <0.1 Ω/sq can be obtained using electrodeposited metal grids. Electrodeposition metal tracks have a higher conductivity metal, i.e. approximately 1.2 times compared several times bulk conductivity for printed Ag-inks, and a higher aspect ratio. As a consequence electrodeposition gives lower transmittance losses due to a lower surface coverage by metal grids. Moreover, the feature sizes <50 μm required for optimal performing grids are near the lower limit of printing techniques, but can easily be achieved by electrodeposition. In [7] grids were made using photolithographic patterning of the ITO followed by electrodeposition. Industrially photolithography is not a viable method for large area grid electrodeposition on flexible foils.

In the last decade it has been shown that soft-lithography techniques present a possible low-cost and industrial viable patterning method down to sub-micron scale. Soft-lithographic patterning, in particular microcontact printing, can be combined with electroless deposition to apply metal patterns as described in [14–19]. Using a patterned stamp patterns of Pd-seeds [14, 18, 19], of self-assembling molecules (SAM) on Pd-catalysed substrates [15, 16, 19] and of a SAM based etching mask on a Pd-film [17] have been microcontact printed on silicon, glass and polymer substrates followed by electroless deposition. Microcontact printing of inhibiting SAMs on Pd-seeds is the most suitable for interconnection in opto-electronic applications. For the required low surface coverage by the metal tracks subtractive etching of a metal film is very material inefficient and printing of Pd-seeds is limited by the mechanical integrity of soft silicone stamps.

Although the inhibition of electroless deposition by long-chain carbon thiol and siloxane SAMs printed on Pd-seeds has been shown, the electrochemical phenomena underlying the inhibition have not been widely studied. In this article, an investigation into the electrochemical reactions involved in the inhibition of electroless Ni deposition on Pd-seeds by thiol SAMs is reported. Interestingly, it was found that similar inhibition of electroless deposition can also take place on ITO by hexadecylamine (HDA) SAMs. The activation and blocking of electrochemical active sites on ITO is described.

2 Experimental details

Polarisation and cyclic voltammetry measurements were performed using an Autolab PGSTAT 20 potentiostat (Eco Chemie B. V., Utrecht, The Netherlands). Chronoamperometry and chronopotentiometry measurements were performed using an Iviumstat Electrochemical Interface (Ivium Technologies B. V., Eindhoven, The Netherlands). In all experiments a three-electrode set-up was used with a platinum wire counter electrode and a Ag/AgCl (3 M KCl) reference electrode. All potentials are given with respect to this reference. For the electrochemical measurement on Pd-seeds an Autolab rotating disc electrode (RDE) (Metrohm Autolab B. V., Utrecht, The Netherlands) with a 7 mm^2 platinum electrode tip was used as working electrode. Preliminary experiments showed that optimal electroless Ni layers were obtained under stagnant conditions, so the RDE was operated without rotation. After each measurement the Pt-RDE was cleaned by subsequent immersion for 10 min in 35 % HNO_3 in water for the removal of Ni and for 10 min in 18.5 % HCl in water for the removal of palladium and rinsed with demineralised water and dried. If necessary, the procedure was repeated until the electrode surface was completely clean. Immediately before each measurement Pt-RDE was cleaned with ethanol.

The Pd-seeds were deposited on the Pt-RDE by contacting the Pd-surface with a droplet of a solution of 0.053 M of $SnCl_2$ and 0.4 M HCl in demineralised water for 2 min, followed by a solution of 0.0014 M $PdCl_2$ in 0.025 M HCl in demineralised water for 1 min. After both steps the electrode was thoroughly rinsed with demineralised water and dried. A commercial (two component) solution (Enplate^{TM} EN-439 E, Enthone Inc.) was used for the electroless Ni deposition on the Pd-catalysed Pt-RDE. The solution was prepared by mixing of 60 ml l^{-1} of component A and 150 ml l^{-1} of component B in demineralised water. The solution contains 0.1 M of Ni^{2+} and 0.26 M $NaPO_2H_2 \cdot H_2O$ as reducing agent and was operated at 90 °C and pH 4.9. For the cyclic voltammetric determination of the inhibitor molecule adsorption on the Pd-seeds a ferro/ferri cyanide indicator redox couple was used. A solution of 0.002 M $K_4Fe(CN)_6$ and 0.002 M $K_3Fe(CN)_6$ was prepared in a buffer solution of 0.1 M Na_2HPO_4 and 0.1 M KH_2PO_4 of pH 6.5.

50 Ω/sq ITO coated PET-foil (Southwall Technologies, UK) was used as working electrode for inhibitor tests on ITO. The ITO was ultrasonically degreased in iso-propanol for 5 min followed by ultrasonic cleaning in 15 % HNO_3 for 3 min. An electroless Ni solution containing 0.1 M $NiSO_4 \cdot 7H_2O$, 0.3 M lactic acid, 0.18 M CH_3COONa and 0.042 M dimethylammino borane (DMAB) was used. The solution operated at pH 6.1 and 50 °C. It was found that this solution directly deposited Ni on the ITO without the need for surface activation by Pd-seeds. To obtain a good ohmic contact it was contacted outside the measurement cell using copper foil. Ohmic losses due to the non-zero resistance of the ITO were minimized by limiting the active electrode area to 1 cm^2. Electrochemical impedance spectroscopy measurements were done at high frequency to determine the ohmic loss in the set-up with the ITO working electrode. Typically a resistance of 10 Ω including the ohmic loss

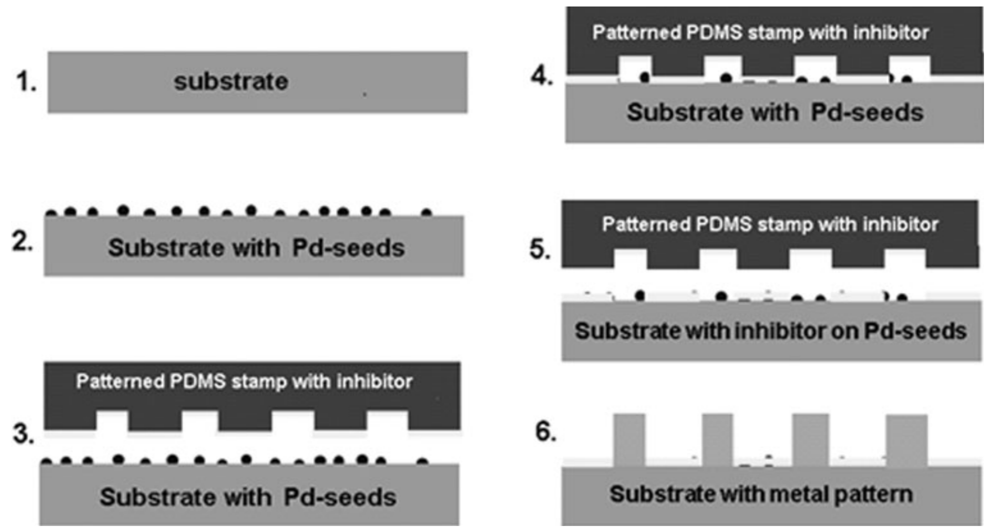

Fig. 1 Schematic picture of microcontact printing of inhibitors for patterned electroless deposition showing: *1* A non-conducting substrate, *2* surface activation by catalytic Pd-seeds, *3* a patterned stamp loaded with inhibitors, *4* transfer of inhibitors from the stamp to the substrate, *5* substrate with a pattern of active and inhibited Pd-seeds, *6* substrate with a pattern of metal tracks

between the reference electrode tip and the ITO working electrode was found. Polarization curves were corrected for the ohmic drop, but for the low current density range (<25 A m^{-2}) investigated it is mostly negligible.

The inhibitors were either deposited by immersion or by microcontact printing. For most electrochemical measurements on Pd-seeds, the Pt-RDE was dipped in a 0.01 M solution of the inhibitor in ethanol for 5 s. After dipping, the Pt-RDE was dried, rinsed with demineralised water and dried again. A flat or patterned polydimethyl siloxane (PDMS) stamp was immersed for 1 min in a 0.01 M solution of the inhibitor in ethanol for microcontact printing. The PDMS stamp was rinsed with ethanol and dried after which the stamp was put in conformal contact with the Pt-RDE electrode or the ITO substrate. After 1 min the stamp was peeled off and the substrate was rinsed with demineralised water and dried. The PDMS stamp was prepared by pouring two component Sylgard® 184 silicone elastomer (Dow Corning) mixed in a 1:10 ratio, degassed in a desiccator, on to a patterned or flat silicon wafer. After drying at 60 °C for 2 h the stamp with a replicated pattern was removed from the master.

3 Results and discussion

3.1 Microcontact printing of inhibitors

In Fig. 1 the microcontact printing of inhibitors for electroless deposition on Pd-catalysed non-conducting substrates, typically polymer foils, is schematically depicted. First the substrate is activated for electroless deposition by application of catalytic Pd-seeds. Although the use of various types of Pd-seeds has been reported [15, 16, 19] the well-known two-step Pd-seeding process used for electroless deposition on plastics can be used. First the substrate is contacted with an acidic Sn^{2+} containing solution, which in the second step reduces Pd^{2+} ions to nanoscale Pd^0 seeds on the substrate. Subsequently, the Pd-seed covered substrate is contacted with a PDMS stamp loaded with inhibitor molecules. The soft PDMS material enables a conformal contact between the stamp and the substrate. The low surface energy of PDMS allows easy and full transfer of inhibitor molecules to the Pd-seeds on the areas where the stamp is in contact with the substrate. After removal of the stamp the substrate contains a pattern of Pd-seeds with and without adsorbed inhibitor molecules. The substrate is transferred to an electroless deposition solution in which electroless metal deposition only occurs on non-inhibited Pd-seeds. After deposition this results in a pattern of metal tracks on the polymer substrate.

In Fig. 1 a patterned stamp is shown, but as an alternative also a patterned substrate can be used. As shown in the electron microscope picture in Fig. 2 in this way metal grids can be embedded in the substrate. Embedded metal grids have the advantage that a planar surface for subsequent deposition of TCO and other layers in thin film devices is obtained. Using photolithography a grid pattern was applied in a photoresist resin coated on PEN foil. After Pd-seeding a flat PDMS stamp loaded with hexadecanethiol (HDT) was used to prevent electroless Ni deposition on the protruding areas and allow electroless Ni deposition in the recess in the photoresist. A pattern of 5 µm wide Ni lines at 95 µm distance is shown in Fig. 2. Using either a patterned PDMS stamp or a patterned foil substrate metal interconnect lines or grids with feature sizes down to 1–20 µm were obtained.

3.2 Inhibition on Pd-seeds

In [15, 16, 19] long-chain carbon thiol or siloxane compounds are described as effective inhibitors for electroless

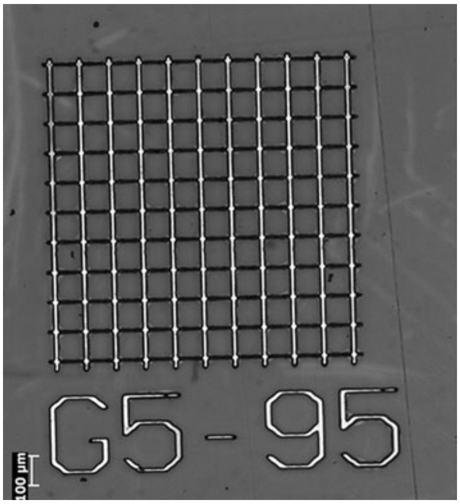

Fig. 2 Electron microscope picture of a grid of 5 μm thick, 5 μm wide Ni lines at 95 μm distance embedded in a 10 μm SU 8 photoresist layer on PEN-foil prepared by microcontact printed HDT inhibitor molecules followed by electroless Ni deposition

deposition by microcontact printing. Extensive literature exists on the self-assembly properties of these long-chain carbon compounds. In particular the formation of self-assembling monolayers of thiol-compounds on gold surfaces has been widely studied. On gold very homogeneous and strongly bond monolayers of SAM can be formed due to the strong covalent bond between sulphur in the thiol-moiety and gold. In [20] the self-assembly of thiol-compounds on Pd-surfaces was studied showing similar SAM structures involving Pd–S bonds as on gold and in particular silver. From the co-ordination chemistry of Pd it is known that Pd-ions form strong complexes with combined N and S groups as present in azole compounds [21]. The azole compounds 2-mercaptobenzothiazole (MBT) and 2-mercaptobenzimidazole (MBI) have been reported to form self-assembling monolayers on gold through their thiol-moiety [22, 23]. Based on these reports and the complexes formed between Pd-ions and MBT in [21]. Figure 3 tentatively depicts the possible co-ordination of MBT and MBI molecules on Pd. MBT is used as a stabiliser to electroless Ni solutions to prevent the spontaneous decomposition of the electroless solution. The stabilizing action results from inhibition of electroless deposition on particulate contaminants or surface heterogeneities by adsorbed MBT molecules. Hence, it can be inferred that microcontact printed MBT and MBI might by very effective inhibitors for patterned electroless deposition. The inhibition of electroless deposition by microcontact printed MBT and MBI on Pd-seeds was investigated and compared to HDT by electrochemical measurements.

Obviously, electrochemical characterisation of Pd-seeds with adsorbed inhibitor is not possible on non-conducting,

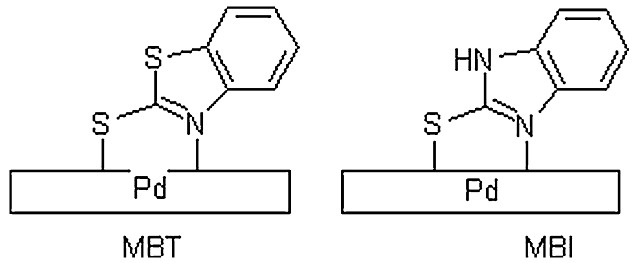

Fig. 3 Tentative picture of the adsorption of MBT and MBI on Pd

e.g. polymer foil, substrates. In contrast to Pd, Pt is not catalytic towards oxidation of hypophosphite, which is the most common reducing agent in electroless Ni deposition solutions. Therefore, a Pt-RDE was used as substrate for potential and current transients and cyclic voltammetry of electroless Ni deposition on (inhibited) Pd-seeds. Figure 4 shows open-circuit potential transients in the EN439 electroless Ni deposition solution at 90 °C measured using the stagnant Pt-RDE with and without Pd-seeds and adsorbed inhibitors. All transients start with a fast decrease in potential from high positive values of 0.2–0.7 V versus Ag/AgCl in the first 2 min. This can be explained by the on-set of diffusion controlled reduction of dissolved oxygen by hypophosphite. After this initial potential decrease the bare Pt-RDE reaches a steady state potential around 0 V versus Ag/AgCl. From the Nernst equation it can be calculated that the equilibrium potential for Ni^{2+} reduction is approximately −0.5 V versus Ag/AgCl using 0.1 M for the Ni^{2+} concentration, 363 K for the temperature, a two electron transfer and a standard equilibrium potential of −0.257 V versus NHE. The 0.5 V more positive potential of the Pt-RDE confirms that no electroless Ni deposition occurs on Pt as it does not catalyse the hypophosphite oxidation.

In contrast the open-circuit transients of Pd-seeded Pt reaches a steady state value around −0.62 V versus Ag/AgCl, i.e. 0.12 V cathodic to the equilibrium potential for Ni^{2+} reduction, resulting in electroless Ni deposition on the electrode. The open-circuit potentials of Pt-surfaces with Pd-seeds dipped or microcontact printed with MBT, MBI or HDT all reach a steady state value within 0.1 V of the 0 V versus Ag/AgCl obtained for bare Pt. Hence, with MBT, MBI and HDT adsorbed on the Pd- seeds the Pt-RDE virtually acts as a bare Pt-electrode. It can be concluded that MBT, MBI and HDT are able to prevent electroless Ni deposition by completely blocking the catalytic activity of Pd-seeds towards hypophosphite oxidation. Figure 4 also shows that one minute microcontact printing of MBT is as least as effective in inhibiting electroless deposition on Pd-seeds as five minutes dipping of Pd-seeds in a 0.01 M MBT solution in ethanol. This suggests that in both cases a strong and very specific bonding interaction between Pd and MBT is created, similar to the formation of self-assembling monolayers.

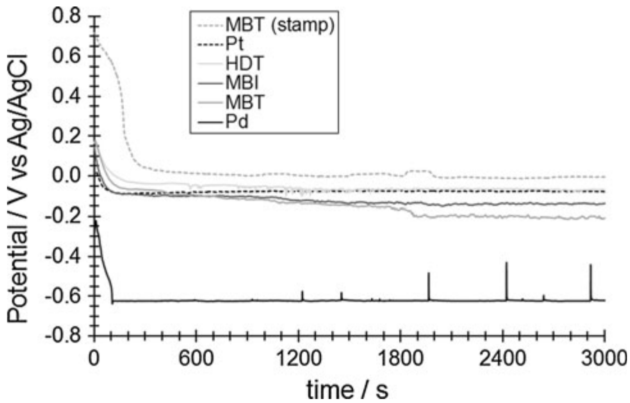

Fig. 4 Open-circuit potential transients on a stagnant Pt-RDE in the EN439 electroless Ni deposition solution at 90 °C. Transients for the bare Pt surface (Pt), Pt with Pd-seeds (Pd) and Pt with Pd-seeds and with HDT (HDT) and MBI (MBI) applied by dipping and with MBT applied by dipping (MBT) and micro-contact printing (MBT (stamp)) are given

Next the type of inhibition by MBT, MBI and HDT, i.e. anodic or cathodic inhibition or both, was investigated using potentiostatic current transients. The variation of the current density in time was measured in the EN439 electroless Ni solution at 91 °C each 0.1 V for potentials between 0 and −0.7 V versus Ag/AgCl for 900 s on a stagnant Pt-RDE seeded with Pd with and without MBT applied by microcontact printing. In all measurements the current density varied in time, but reached practically a steady state after 600 s. In Fig. 5, the polarisation curves for Pd-seeded Pt with and without MBT derived from the measured current transients after 600 s are shown. The current density behaviour in the potential range between 0 and −0.5 V versus Ag/AgCl is high-lighted in more detail in Fig. 5b. It can be seen that in this potential range the current density on the Pd-seeded Pt with MBT is consistently more negative than on Pd-seeded Pt without MBT. At potentials more positive than −0.3 V versus Ag/AgCl the net current density is anodic on the Pd-seeded surface without MBT and cathodic on Pd-seeds with MBT. The net anodic current on the Pd-seeded surface without MBT is caused by the catalytic oxidation of hypophosphite on Pd. At the same time reduction of dissolved oxygen occurs which results in a net cathodic current density at −0.4 and −0.5 V versus Ag/AgCl. When MBT is microcontact printed on the Pd-seeds the oxygen reduction reaction is dominant and the net current density is cathodic in the entire potential range from 0 to −0.5 V versus Ag/AgCl. In the measured transients the cathodic current density decreases in time with an increasingly slower rate indicative for the diffusion controlled reduction of dissolved oxygen. This clearly demonstrates that MBT inhibits oxidation of the reducing agent hypophosphite on Pd-seeds in the electroless Ni solution.

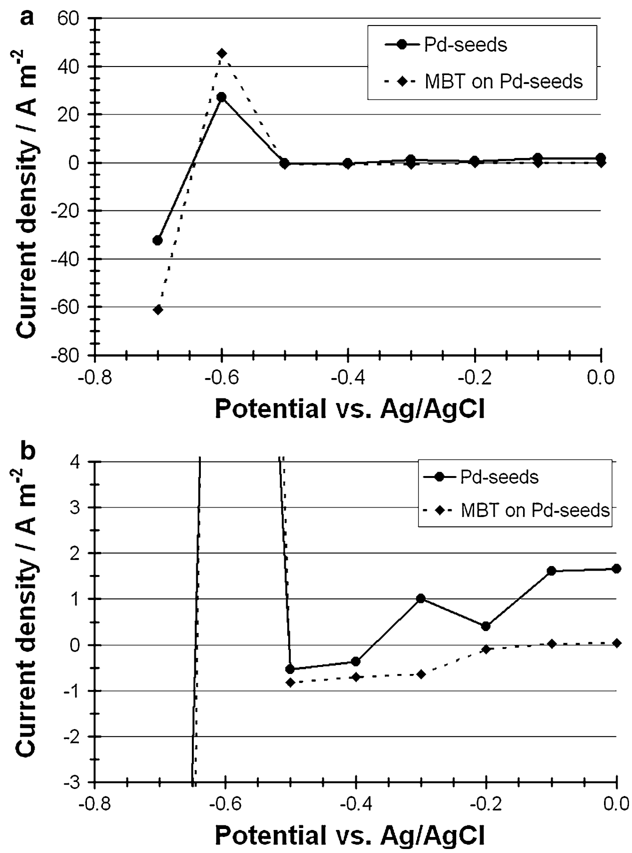

Fig. 5 Polarisation curves in the EN439 electroless Ni solution at 91 °C.on a stagnant Pt-RDE seeded with Pd with and without MBT applied by microcontact printing. The current density was taken from the potentiostatic current transients after 600 s. The full potential range of 0.1 V intervals from 0 and −0.7 V versus Ag/AgCl is shown in (**a**). The current density behaviour in the potential range between 0 and −0.5 V versus Ag/AgCl is high-lighted in more detail in (**b**)

As mentioned the equilibrium potential for Ni^{2+} reduction in the electroless Ni plating solution is −0.5 V versus Ag/AgCl. Hence, at −0.6 and −0.7 V versus Ag/AgCl Ni deposition can take place. At −0.7 V versus Ag/AgCl this is evidenced by the net cathodic current density and by visual observation of Ni on the electrodes after the measurements. Also at −0.6 versus Ag/AgCl a Ni deposit of several microns was observed on the electrode surfaces despite the high net anodic current density measured at this potential. This is caused by a strong increase in the catalytic surface area for hypophosphite reduction by deposited Ni as electroless Ni deposition is an autocatalytic process. In correspondence with the open-circuit potential transient for Pd-seeded Pt in Fig. 4 the net current equals zero around −0.62 V versus Ag/AgCl. At these potentials more cathodic than −0.5 V versus Ag/AgCl there is only a minor difference in the polarisation behaviour between Pd-seeded Pt with and without MBT that falls within the experimental variation of the current transient measurements. It can thus be concluded that MBT does not prevent the reduction of

Ni^{2+} on Pd-seeds, but inhibits electroless Ni deposition by specifically inhibiting the oxidation of hypophosphite on Pd-seeds.

In contrast HDT was found to inhibit both the Ni^{2+} reduction and hypophosphite oxidation on Pd-seeds. In current transient on Pd-seeded Pt with microcontact printed HDT (data not shown) the same dominance of dissolved oxygen reduction was found at potentials more anodic than −0.5 V versus Ag/AgCl. However, at −0.6 and −0.7 V versus Ag/AgCl no Ni was observed on the RDE after 900 s in the electroless Ni solution. Instead of Ni deposition hydrogen gas formation was observed at these potentials. From the current transients it can be concluded that both MBT and HDT effectively inhibit electroless Ni deposition on Pd-seeds, but MBT only through anodic inhibition of hypophosphite oxidation and HDT through both cathodic and anodic inhibition.

The difference in type of inhibition between HDT and MBT suggests a different adsorption of these inhibitors on Pd-seeds. Cyclic voltammetry measurements in a 0.002 M ferro/ferri cyanide solution buffered at pH 6.5 using a phosphate buffer were performed to investigate the adsorption behaviour of both inhibitors. Ferro/ferri cyanide is frequently used as a reversible redox couple to determine the adsorption behaviour of SAMs on metallic surfaces [22, 23]. From the difference in peak current densities and the consumed charge in cyclic voltammetry scans between bare and SAM covered electrode surfaces the surface coverage by SAMs can be calculated. Figure 6 shows cyclic voltammograms measured between 0.5 and −0.05 V versus Ag/AgCl with a step potential of 0.01 V, a scan rate of 0.025 V/s starting in the cathodic direction on the Pt-RDE with and without Pd-seeds and with and without microcontact printed MBT and HDT. In Fig. 6a it can be seen that on Pt the well-defined anodic and cathodic peaks characteristic of the reversible ferri/ferro cyanide redox couple are obtained. It follows from this figure that HDT completely inhibits the ferro/ferri cyanide reaction indicating strong adsorption of HDT on Pt. In contrast microcontact printed MBT leads to a small reduction in the anodic and cathodic peak current densities only, signifying a much lower surface coverage by adsorbed MBT.

The same cyclic voltammetry measurements for Pd-seeded Pt are presented in Fig. 6b. In contrast to bare Pt a well-defined voltammogram for the ferro/ferri cyanide couple is not obtained on the Pd-seeded Pt. A highly irreversible reaction involving considerably lower current densities, most probably reduction of dissolved oxygen, dominates on the Pd-seeds. Various alternative redox couples, i.e. Fe^{3+}/Fe^{2+}, Cu under potential deposition and ferro/ferri cyanide at pH 4.9, were tested, but none yielded satisfactory voltammograms. To determine if the suppression of the ferro/ferri cyanide reaction originates from the

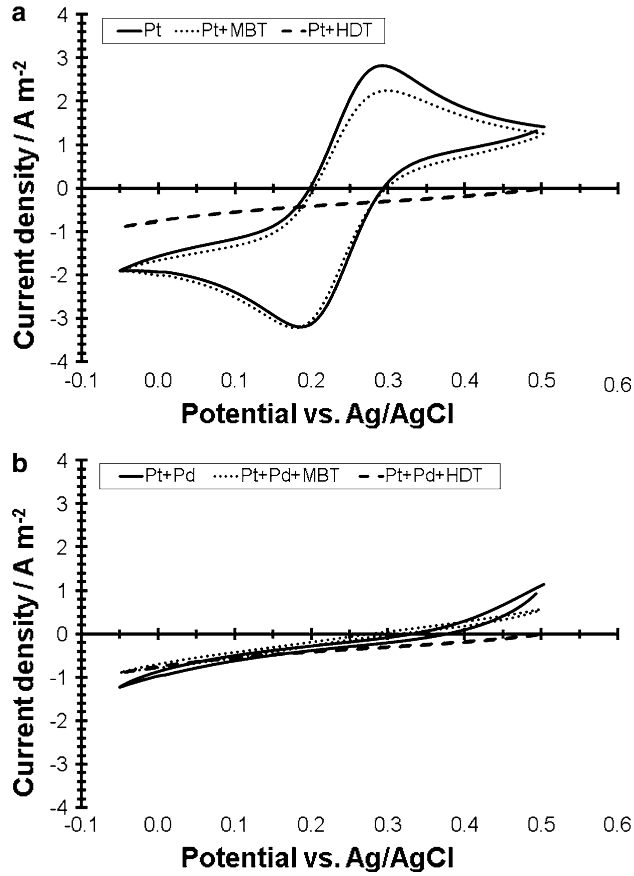

Fig. 6 Cyclic voltammograms measured between 0.5 and −0.05 V versus Ag/AgCl with a step potential of 0.01 V, a scan rate of 0.025 versus starting in the cathodic direction on the Pt-RDE without (**a**) and with (**b**) Pd-seeds and with and without microcontact printed MBT and HDT

nanoparticle nature of the Pd- seeds or from the inherent Pd-electrochemical activity, cyclic voltammograms were measured on the Pt-RDE coated with a 4 μm Pd-electrodeposited film. Although to a lesser extent also on the Pd-film the ferro/ferri cyanide couple was strongly suppressed resulting in a poorly defined cyclic voltammogram. Hence, the electrochemical activity of Pd seems to prevent the measurement of cyclic voltammograms suitable for accurate determination of the MBT and HDT surface coverage.

However, as shown in Fig. 6 an inhibiting effect of HDT and MBT on Pd-seeded Pt resulting in a decreased anodic current density can still be observed. In order to get an estimate of the surface coverage of these compounds on Pd-seeds the relative surface area coverage by HDT and MBT was calculated from the peak current density at 0.3 V versus Ag/AgCl on Pt and at 0.5 V versus Ag/AgCl on Pd-seeds and the Pd-layer. The estimated surface coverages of microcontact printed MBT and HDT on Pt, Pd-seeded Pt and the 4 μm Pd-layer are given in Table 1. From these estimates it can be seen that surface coverage of HDT is

Table 1 Surface coverage of MBT and HDT on Pt, Pd-seeds and a Pd-layer estimated from the peak current density at 0.3 V versus Ag/AgCl on Pt and at 0.5 V versus Ag/AgCl on Pd-seeds and layer measured in the cyclic voltammograms shown in Fig. 6

Substrate	Peak current density (A m^{-2})			Surface coverage (%)	
	Pt	Pt + MBT	Pt + HDT	MBT	HDT
Pt	3.50	2.92	0.28	17	92
Pd-seeds	0.84	0.51	−0.03	39	100
Pd-layer	1.24	0.82	0.56	34	55

considerably higher than the surface coverage by MBT for all three surfaces. The most accurate estimate is for Pt, where well-defined voltammograms were measured, indicating practically complete surface coverage by HDT and only about one-fifth for MBT. Combined with the difference in inhibition type determined from the current transients discussed above this suggests a different adsorption mechanism of MBT and HDT. HDT seems to form a well-ordered self-assembling monolayer that completely inhibits electrochemical activity of Pt and probably also of Pd-seeds. In contrast MBT seems to adsorb to specific surface sites only giving limited inhibition on Pt, but enabling specific inhibition of hypophosphite oxidation on Pd-seeds. However, further investigation is needed to verify this hypothesis.

3.3 Inhibition on ITO

The discussed results prove that microcontact printing of inhibitors is a viable method for the application of metal grids on polymeric foils. In opto-electronic devices metal grid covered polymeric foil can serve as substrate for TCOs and subsequent thin films. However, for certain thin film devices deposition of a metal grid on top of the TCO is more practical. Therefore, the possibility to deposit metallic grids on ITO using a microcontact printed inhibitor was explored. Obviously, the same microcontact printing method shown in Fig. 1 for polymeric foils might be used by first applying Pd-seeds on the ITO surface [24]. Suprisingly, it was found that electroless Ni deposition can take place directly onto 50 Ω/sq ITO on PET-foil using a neutral, i.e. pH 6.1, electroless Ni solution at 50 °C containing DMAB as reducing agent. Several other electroless Ni solutions were tested, among others the hypophosphite based EN439 solution used for the Pd-seeded substrates, but none autocatalytically deposited nickel on ITO. It was found that deposition of well-adherent electroless Ni was only possible after a three minute pre-treatment of the ITO substrate in 15 % HNO_3. Pre-treatment in other acids, i.e. HCl, H_3PO_4, H_2SO_4 and oxalic acid, did not result in the same well-adherent electroless Ni layer on ITO. Cathodic polarisation curves measured in the electroless nickel solution without reducing agent indicate that after the pre-treatment in HNO_3 the crystallisation overpotential for nickel deposition on ITO is reduced by approximately 100 mV. Pre-treatment in the other acids does not affect or even increases the crystallisation overpotential for nickel deposition. Surface characterisation of the ITO substrate before and after treatment in 15 % HNO_3 shows that the surface roughness and sheet resistance do not change due to the HNO_3 treatment. Only the contact angle with water decreases from 55° to 22°. This indicates that despite the strong acidity the 15 % HNO_3 solution does not significantly etch the ITO surface, but does create a more hydrophilic surface.

Functionalization of ITO surfaces by self-assembling molecules has been reported in for example [25–28]. Long chain alkanes functionalized with among others, alkoxy silane [25, 27, 28] carboxylic acid, or amine end-groups [25, 26] have been shown to form self-assembling monolayers on ITO. In this study HDA was tested as an inhibitor for electroless nickel deposition on ITO. Figure 7 shows cathodic polarisation curves measured in the electroless nickel solution without DMAB on pre-treated ITO after immersion in a 0.01 M HDA solution in ethanol for various times and after microcontact printing of HDA. On the ITO substrate without HDA in the forward scan reduction of dissolved oxygen starts at −0.7 V versus Ag/AgCl. After diffusion limitation of the oxygen reduction Ni^{2+} reduction commences around −0.8 V versus Ag/AgCl. When HDA is adsorbed on the ITO surface the reduction of dissolved oxygen is inhibited and the start of the Ni^{2+} reduction is shifted to more negative values. In the most extreme case, after 25 h immersion in the HDA solution, the start of Ni^{2+} reduction is shifted by 100 mV to approximately −0.9 V versus Ag/AgCl. It can be concluded that HDA adsorption increases the crystallisation overpotential for Ni deposition on ITO to about the same value as non pre-treated ITO. As it was determined that electroless nickel deposition on the ITO substrate takes place at a potential of −0.85 V versus Ag/AgCl HDA is able to inhibit electroless Ni deposition on ITO. The effect of microcontact printed HDA on the nickel crystallisation overpotential on ITO is smaller than by immersion in the HDA solution as can be seen in Fig. 7. Nevertheless preliminary test show that microcontact

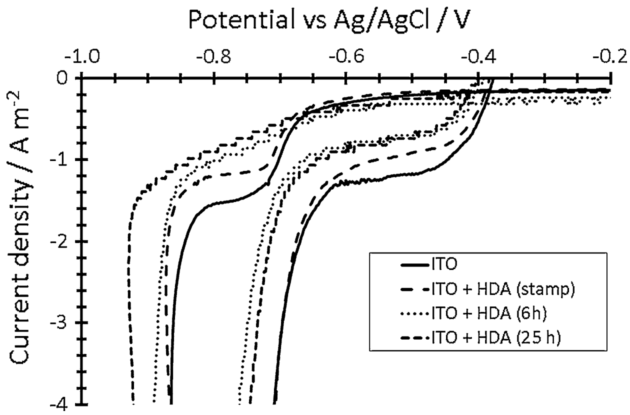

Fig. 7 Polarisation curves in the DMAB based electroless Ni solution at 50 °C on 50 Ω/sq ITO on PET-foil with and without HDA applied by immersion in a 0.01 M solution in ethanol for various time or by microcontact printing. Both the forward scan (*left curve*) and backward scan (*right curve*) are shown in each case

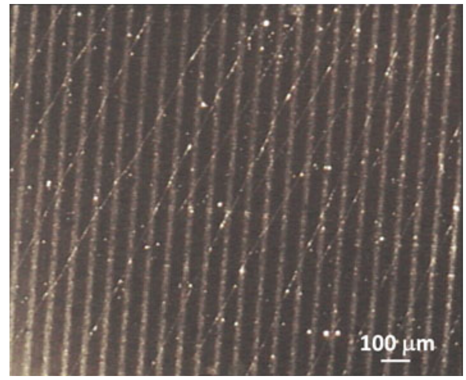

Fig. 8 Optical microscope picture of a grid of 1 µm thick, 50 µm wide Ni lines at 50 µm distance on 50 Ω/sq ITO on PET-foil prepared by microcontact printed HDA inhibitor molecules followed by electroless Ni deposition

printing using a patterned PDMS stamp loaded with HDA enables patterned electroless nickel deposition on ITO. Figure 8 shows an optical microscope picture of a grid of 50 µm wide Ni lines on 50 Ω/sq ITO on PET-foil prepared by microcontact printed HDA followed by electroless Ni deposition.

It can be seen in Fig. 7 that the longer the immersion time in the HDA solution the larger the shift in the nickel crystallisation overpotential. As self-assembly processes typically take several hours to form well-ordered monolayers, this indicates that HDA indeed self-assembles on the ITO surface. The nature of the catalytic activity of ITO for electroless nickel deposition in the neutral DMAB based solution was not investigated in detail. However, based on literature data and the reported results a hypothesis for the inhibition of electroless nickel deposition on ITO by HDA can be inferred. In [25] it is concluded from XPS data that the amine group in HDA forms a Lewis base–acid bond with tin sites on the ITO surface. The inhibited nickel deposition by adsorbed HDA thus indicates that tin sites are the active sites for electroless nickel deposition. The polarisation curves show that the inhibition is related to a negative shift in the crystallisation overpotential to that of the ITO surface before HNO_3 pre-treatment. Hence, the activation pre-treatment in 15 % HNO_3 solution seems to either create or expose the tin sites where HDA adsorbs. Indeed in [29] it is reported that acid etching exposes tin-rich near surface sites by removing a surface film of indium hydroxides and carbonates that covers ITO surfaces. It is hypothesized that these exposed tin-rich surface sites constitute crystalline SnO_x deposits with $x < 2$ that enhance the electro-activity of ITO. It seems likely that these electrochemically active low-valence tin sites reduce the crystallisation overpotential for nickel deposition thereby facilitating electroless nickel deposition on ITO. Similarly, for SnO_2 it was shown that the formation of low valence tin sites enhances the electrodeposition and adhesion of copper [30]. It can be speculated that a reducing action of lower valence tin, similar to the Sn^{2+} sensitisation in Pd-catalyst deposition on non-conducting substrates, enables Ni nucleation on ITO. However, more in depth investigation is needed to establish if this hypothesised mechanism of electro-active low valence tin sites is responsible for the observed acid activation and HDA inhibition of electroless nickel deposition on ITO.

4 Conclusions

Using various electrochemical measurements techniques it was shown that microcontact printed inhibitors are able to locally prevent electroless deposition on Pd-seeds and ITO. Open-circuit potential measurements combined with potentiostatic current transients show that adsorption of MBT on Pd-seeds inhibits the hypophosphite oxidation in an electroless nickel solution, thereby preventing electroless nickel deposition. HDT has the same inhibiting effect on hypophosphite oxidation, but also inhibits the Ni^{2+} reduction on Pd-seeds. Cyclic voltammetry measurements suggest that this difference is related to a different adsorption mechanism of HDT and MBT on Pd-seeds. HDT seems to form a self-assembling monolayer that completely blocks the electrochemical reactions, whereas MBT adsorbs only on specific electrochemical active sites. Similarly, polarization measurements showed that after a pre-treatment in HNO_3 HDA is able to inhibit electroless Ni deposition on ITO coated on PET-foil. The pre-treatment in HNO_3 activates the ITO surface for electroless Ni deposition by reducing the nickel crystallisation overpotential. HDA forms a self-assembling monolayer that inhibits Ni^{2+} reduction on ITO

by increasing the crystallization overpotential for Ni electrodeposition by approximately 100 mV.

References

1. Hovestad A, Rendering H, Peter M, Meinders ER (2010) Proceedings of the 8th international conference on coatings on glass and plastics, p 77
2. Wang X, Zhi L, Múllen K (2008) Nano Lett 8:323
3. De S, Lyons PE, Sorel S, Doherty AM, King PJ, Blau WJ, Nirmalraj PN, Boland JJ, Scardaci V, Joimel J, Coleman JM (2009) ACS Nano 3:714
4. Zhou Y, Hu L, Grüner G (2006) Appl Phys Lett 88:1–123109
5. Bernède JC, Berredjem Y, Cattin L, Morsli M (2008) Appl Phys Lett 92:1–083304
6. Rim YS, Kim SM, Jap KH (2008) J Appl Phys 47:5022
7. van Deelen J, Rendering H, Hovestad A (2012) Materials research society symposium proceedings, vol 1323, p 17
8. Kessler J, Wennerberg J, Bodegård M, Stolt L (2003) Sol Energy Mater Sol Cells 75(35):35
9. Tvingstedt K, Inganäs O (2007) Adv Mater 19:2893
10. Kang M-G, Park HJ, Ahn SH, Guo LJ (2010) Sol Energy Mater Sol Cells 94:1179
11. Kang M-G, Kim M-S, Kim J, Guo LJ (2008) Adv Mater 20:4408
12. Lee J-Y, Connor ST, Cui Y, Peumans P (2008) Nano Lett 8:689
13. Gosh DS, Chen TL, Pruneri V (2010) Appl Phys Lett 96:041109
14. Hidber PC, Helbig W, Kim E, Whitesides GM (1996) Langmuir 12:1375
15. Bessueille F, Gout S, Cotte S, Goepfert Y, Léonard D, Romans M (2009) J Adhes 85:690
16. Sugimura H, Hanji T, Takai O, Masuda T, Misawa H (2001) Electrochim Acta 47:103
17. Carvalho A, Geissler M, Schmid H, Michel B, Delamarche E (2002) Langmuir 18:2406
18. Hendricks TR, Dams EE, Wensing ST, Lee I (2007) Langmuir 23:7404
19. Geissler M, Kind H, Schmidt-Winkel P, Miche B, Delamarche E (2003) Langmuir 19:6283
20. Love JC, Wolfe DB, Haasch R, Chabinyc ML, Paul KE, Whitesides GM, Nuzzo RG (2003) J Am Chem Soc 125:2597
21. Banerji S, Byrne RE, Livingstone SE (1982) Trans Metal Chem 7:5
22. Shervedani RK, Babadi MK, Hatefi-Mehrjardi A (2007) Electrochim Acta 52:7051
23. Donneux Th, Buess-Herman Cl, Lipowski J (2004) J Electroanal Chem 564:65
24. Kim JJ, Cha SH (2002) Jpn J Appl Phys 40:L1269
25. Bermudez VM, Berry AD, Kim H, Pique A (2006) Langmuir 22:11113
26. Oh S-Y, Yun Y-J, Kim D-Y, Han S-H (1999) Langmuir 15:4690
27. Koide Y, Such MW, Basu R, Evmenenko G, Cui J, Dutta P, Hersam MC, Marks TJ (2003) Langmuir 19:86
28. Oh S-Y, Yun Y-J, Hyung K-H, Han S-H (2004) New J Chem 28:495
29. Brumbach MP, Veneman PA, Marrikar FS, Schulmeyer T, Simmons A, Xia W, Lee P, Armstrong NR (2007) Langmuir 23:11089
30. Liu JS, Laverty SJ, Maguire P, McLaughlin J, Molloy J (1994) J Electrochem Soc 141:L38